Solid-State Electronics 198 (2022) 108470

Contents lists available at ScienceDirect

Solid State Electronics

journal homepage: www.elsevier.com/locate/sse

Calculation of the mobility in Al_2O_3/GaN electron channel: Effect of p-doping and comparison with experiments☆

Bledion Rrustemi [a,b,*], François Triozon [a], Marie-Anne Jaud [a], William Vandendaele [a], Gérard Ghibaudo [b]

[a] Univ. Grenoble Alpes, CEA, LETI, F-38000 Grenoble, France
[b] Univ. Grenoble Alpes, IMEP-LAHC Minatec, F-38000 Grenoble, France

ARTICLE INFO

Keywords:
Al_2O_3/GaN
Electron mobility
p-doping

ABSTRACT

The low field electron mobility of Al_2O_3/GaN channel is calculated using a semi-classical framework. The aim is to obtain the mobility as a function of the electron sheet density and the temperature, with different p-doping conditions in GaN, and to compare it with our measurements on various samples. The scattering with bulk and surface phonons is taken into account. Scattering with dopants, interface charges, neutral impurities and interface roughness is also included in an attempt to account for experimental observations. We found that, when bringing p-dopants closer to the Al_2O_3/GaN interface, the mobility decreases mainly because the electron channel is more confined and located closer to Al_2O_3, thereby enhancing scattering mechanisms located near the Al_2O_3/GaN interface. Our results suggest that most of transport limitations come from Al_2O_3 oxide.

1. Introduction

Due to their wide band gap, high breakdown voltage and good transport properties, GaN is an attractive material for high power/frequency applications. Normally-OFF operations can be achieved with MOS-HEMT architecture which is considered as a promising candidate thanks to its low leakage current [1]. In this context, investigating the transport limitations in Al_2O_3/GaN channel is important for optimizing the performances but also to feed TCAD simulations with physical models. Moreover, the effect of p-doping of GaN on the electron mobility in Al_2O_3/GaN channel has not been reported in literature.

2. Experimental setup

GaN is grown on p-type Si substrate using MOCVD deposition. Transition layers are used for strain management and are followed by a thick and highly Carbon-doped GaN layer (GaN:C, [C] ≈ 2.10^{19} cm^{-3}) to ensure vertical insulation. Then, the GaN channel has either no intentional doping (NID) or is p-doped with Magnesium (Mg). Al_2O_3 oxide is 30 nm thick and is deposited by Atomic Layer Deposition method. The four samples measured are shown in Fig. 1a. Sample A has no Mg-doping and samples B, C and D only differ by the Mg-doping profile $N_A(z)$ below the Al_2O_3/GaN interface (Fig. 1b). Measurements of the low field mobility as a function of the electron sheet density n_s for temperatures ranging from 298 K to 423 K have been performed with split-CV method on transistors with long gate length $L_G = 60$ µm to avoid any effect of access resistances. The electron sheet density is obtained by integrating the gate-to-channel capacitance $C_{GC}(V_G)$ measurement:

$$n_s(V_G) = \frac{1}{e}\int_0^{V_G} C_{GC}(V)dV \tag{1}$$

The effective mobility is then obtained using the split-CV formula:

$$\mu_{eff} = \frac{L_G}{e\,W_G\,V_D}\frac{I_D(V_G)}{n_s(V_G)} \tag{2}$$

where V_D is set to 50 mV to be in low field regime and the gate width W_G is 200 µm. The drain current $I_D(V_G)$ and the gate-to-channel capacitance $C_{GC}(V_G)$ measurements are simultaneous and fast (the total measurement time is 0.7 ms) to avoid gate voltage stress. The protocol is explained in detail and validated in [2].

3. Calculations

The electron density and potential along the stacks are obtained with self-consistent 1D Schrödinger–Poisson simulations for the Γ-valley electrons under the effective mass approximation for non-parabolic and spherical energy bands ($m_{\Gamma M} = m_{\Gamma K} \approx m_{\Gamma A}$ [3]). Non-parabolic

☆ The review of this paper was arranged by Francisco Gamiz.

* Corresponding author at: Univ. Grenoble Alpes, CEA, LETI, F-38000 Grenoble, France.
E-mail address: bledion.rrustemi@cea.fr (B. Rrustemi).

https://doi.org/10.1016/j.sse.2022.108470

Available online 9 October 2022

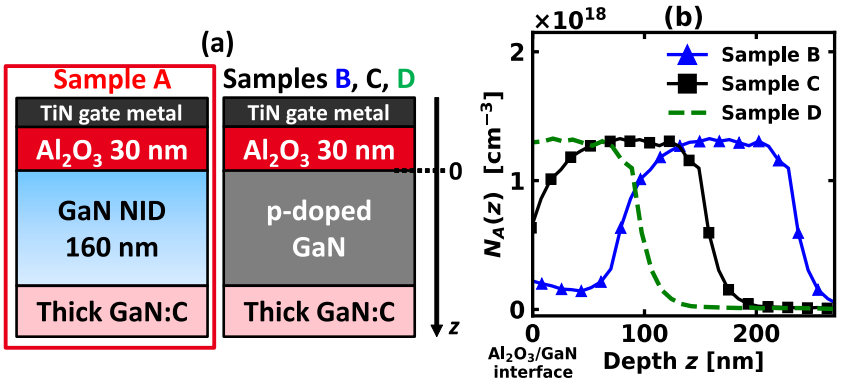

Fig. 1. (a) Stacks studied (NID: Not intentionally doped). (b) $N_A(z)$ profiles (experimental SIMS data). As can be seen from the $N_A(z)$ profiles, p-doped GaN is approximately 260 nm thick in sample B, 160 nm thick in sample C, and 100 nm thick in sample D.

corrections are included using Jin et al. model [4]. Incomplete ionization model is used to properly account for the Fermi level in GaN:C. Carbon impurities are assumed as deep acceptors (0.8 eV above the valence band maximum VBM) partially compensated by shallow donors (0.1 eV below the conduction band minimum) [5]. This leads to a Fermi level pinning at 0.84 eV from the VBM in GaN:C which is consistent with experimental findings [6]. The p-doping is included by using $N_A(z)$ profiles (Fig. 1b) in the simulations, also accounting for incomplete ionization with an Mg acceptor level located at 0.16 eV above the VBM [7]. The framework used to calculate the mobility is based on the linearized 2D Boltzmann transport equation and on Fermi's golden rule. It has been massively used in MOS inversion layers [8–10]. The originality of our study comes from applying this framework in Al_2O_3/GaN channel, from including neutral impurities and from emphasizing the effect of p-doping.

The scattering rates are obtained with Fermi's golden rule. For the elastic scattering mechanism s, the scattering rate of an electron of subband i and energy E is given by:

$$\frac{1}{\tau_i^s(E)} = A\frac{m_\Gamma}{2\pi\hbar^3}\sum_{j|E_j<E}(1+2\alpha(E-U_j))\times\int_0^{2\pi}d\theta(1-cos\theta)|M_{ij}^s(q)|^2 \quad (3)$$

where A is the area, α is the non parabolicity factor and U_j is the expected value of the potential energy of subband j in the confinement direction z [4]. θ is the angle between $\mathbf{k}$ and $\mathbf{k}'$ which are the 2D wavevectors before and after the scattering event, respectively, and $q = |\mathbf{k}-\mathbf{k}'|$. M_{ij}^s is a scattering matrix element, obtained from the 2D Fourier transform of the scattering potential ($V^s(q,z)$) and the wavefunctions (ψ) [9]. For inelastic scatterings (optical phonons), the scattering rates are given by:

$$\frac{1}{\tau_i^{POP,SO}(E)} = A\frac{m_\Gamma}{2\pi\hbar^3}\sum_{j|E_j<E\pm\hbar\omega}\frac{1-f(E\pm\hbar\omega)}{1-f(E)}(1+2\alpha(E\pm\hbar\omega-U_j)) \times\int_0^{2\pi}d\theta(1-cos\theta)|M_{ij}^{POP,SO}(q)|^2 \quad (4)$$

where $\hbar\omega$ is the energy of the optical phonons, + is for the absorption and - is for the emission of a phonon. After calculating the scattering rates of all mechanisms considered, the total scattering rate is obtained using Matthiessen's rule ($1/\tau_i(E) = \sum_s 1/\tau_i^s(E)$). The mobility is finally computed with "Kubo–Greewood" formula:

$$\mu = \frac{-e}{\pi\hbar^2 n_s}\sum_i\int_{E_i}^{\infty}dE\,\tau_i(E)\frac{df^0}{dE}\frac{(E-E_i+\alpha(E-U_i)^2)}{1+2\alpha(E-U_i)} \quad (5)$$

Screening is included by dividing the diagonal scattering matrix elements by the magnitude of the scalar dielectric function [9]. The expressions of the scattering matrix elements of acoustic deformation potential (ADP), piezoelectric potential (PE) and polar optical phonons (POP) are taken from [11]. The effect of surface optical (SO) phonons, which arise from transverse polar optical (TO) mode of Al_2O_3 and GaN, is estimated following the method of Fischetti et al. [12]. Calculations are done assuming an infinite oxide (justified because the oxide is 30 nm thick) and neglecting the coupling with 2DEG's plasmon. Two TO frequencies are considered in Al_2O_3 (ω_{TO1} and ω_{TO2}) and one in GaN (ω_{TO3}). Their value is given in Table 1. Since ω_{TO2} is very close to ω_{TO3}, we assumed $\omega_{TO3} = \omega_{TO2}$ in the calculations. Two SO modes are obtained and their frequency can be expressed as follows:

$$\omega_{SO1}^2 = \omega_{TO1}^2\frac{\epsilon_{ox}^0+\epsilon_{GaN}^0}{\epsilon_{ox}^{int}+\epsilon_{GaN}^0}\ , \quad \omega_{SO2}^2 = \omega_{TO2}^2\frac{\epsilon_{ox}^{int}+\epsilon_{GaN}^0}{\epsilon_{ox}^{\infty}+\epsilon_{GaN}^{\infty}} \quad (6)$$

where ϵ_0, ϵ_{int} and ϵ_∞ refer to the static, intermediate and dynamic permittivity. To calculate the amplitude of these modes, we followed the procedure outlined in [12], that is, for each phonon mode, we calculate the difference in the squared amplitude between the case where the phonon does not respond and the case where the phonon fully responds. Then, the scattering matrix elements can be calculated as in [10].

For SO and POP scatterings, we took into account dynamic screening by including the dependency upon the frequency of phonons in the calculation of the dielectric function as done in [10]. Fig. 2 shows the impact of screening on POP scattering by comparing the POP limited mobility vs n_s in the unscreened, statically screened and dynamically screened cases. As n_s increases, the plasma frequency of the 2D electron channel increases and becomes superior to the frequency of POP such that electrons can more effectively screen the time-dependent POP potential. This is why, when n_s is close to $10^{13}\,cm^{-2}$, the dynamic screening case becomes equivalent to the static screening case. This demonstrates the importance of including dynamic screening to accurately assess the POP limited mobility. Fig. 3 compares all the phonons limited mobilities, highlighting the dominance of POP. The total phonon limited mobility is also shown and it is slightly above $1000\,cm^2\,V^{-1}\,s^{-1}$, which is much higher than the experimental effective mobility, indicating that phonons are far from being the main scattering mechanisms limiting transport.

To account for experimental observations, scattering with dopants, interface charges (ICs) and interface roughness (IR) is included following the approaches which have been employed in bulk MOSFET [9].

Table 1
Material parameters used in the calculations.

	E_G (eV)	m_Γ (m_0)	α (eV^{-1})	ϵ^0 (ϵ_0)	ϵ^∞ (ϵ_0)	ϵ^{int} (ϵ_0)	ω_{LO} (meV)	ω_{TO_i} (meV)
GaN[a]	3.4	0.2	0.186	10.28	5.7	–	92	ω_{TO3} =70
Al_2O_3[b]	7.0	0.4	–	9	3.2	7.27	–	$\omega_{TO1,TO2}$ = 48, 71

[a] E_G, m^Γ from [3]. ϵ^0, ϵ^∞ from [13] and optical modes ω from [14].
[b] E_G, ϵ^0 from [15], effective mass from [16] and the rest from [12,17].
($\epsilon^{int} \approx \epsilon^\infty\,(\omega_{TO2}/\omega_{LO2})^2$ as explained in [12] with ω_{LO2} taken from [17]).

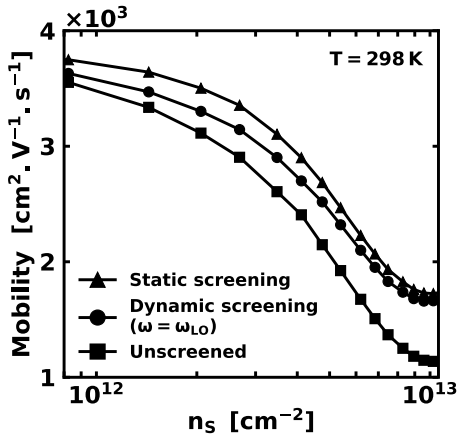

Fig. 2. POP limited mobility vs n_s. Dynamic screening is compared to the unscreened and statically screened cases. (Sample A).

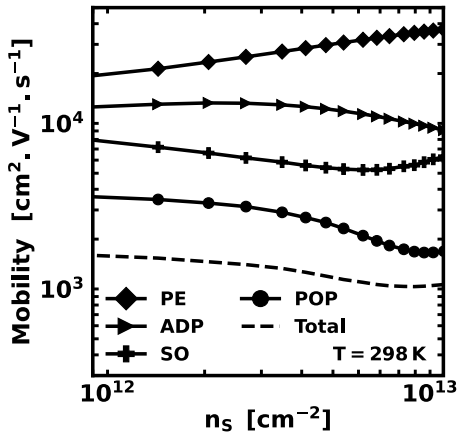

Fig. 3. All phonons limited mobility vs n_s. ADP and PE material properties are taken from [11]. (Sample A).

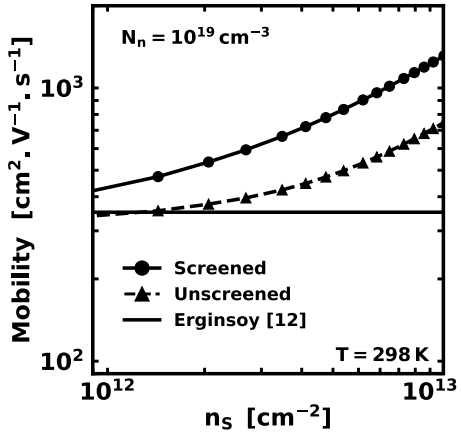

Fig. 4. Neutral impurities limited mobility vs n_s for a uniform density of neutral impurities $N_n = 10^{19}\,\mathrm{cm}^{-3}$ in GaN.

The squared magnitude of the interface roughness scattering matrix elements are obtained from the generalized Prange-Nee term [9]:

$$\left|M_{ij}^{IR}(q)\right|^2 = \left|\int dz\psi_i(z)\psi_j(z)\left(-e\frac{d\phi}{dz}\right) + \left(E_i - E_j\right)\int dz\psi_i(z)\frac{d\psi_j(z)}{dz}\right|^2 |\Delta(q)|^2 \tag{7}$$

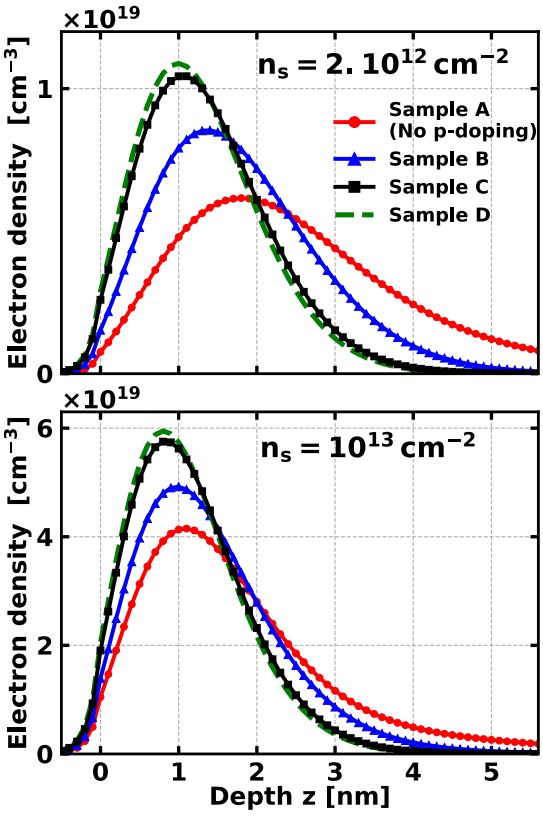

Fig. 5. Electron density vs depth z calculated for the four samples for two different n_s. Top: $n_s = 2.10^{12}\,\mathrm{cm}^{-2}$ and bottom: $n_s = 10^{13}\,\mathrm{cm}^{-2}$. $N_A(z)$ profiles in Fig. 1b are used in the calculations.

where ϕ is the potential and ψ_i, ψ_j are the wavefunctions of subbands i and j, respectively. The roughness is described with an exponential spectrum, $|\Delta(q)|^2$ is given by [9]:

$$|\Delta(q)|^2 = \frac{1}{A}\pi\Delta_{sr}^2\Lambda_{sr}^2\left(1 + \frac{q^2\Lambda_{sr}^2}{2}\right)^{-3/2} \tag{8}$$

where Δ_{sr} is the root-mean-square and Λ_{sr} is the correlation length. The scattering with neutral impurities (NIs) is also included: in addition to non ionized dopants, NIs are added near the Al_2O_3/GaN interface, which will yield a better agreement with experiments. To include this scattering, we use the hydrogen potential scaled by the effective mass and dielectric constant of the medium, as done by Erginsoy [18]. But Erginsoy model is made for 3D transport. In the case of a 2D electron channel, one must consider the non-uniformity of the electron density and the screening produced by the 2D electron gas. We did so by calculating the 2D Fourier transform of hydrogen potential, using the 3D Fourier transform given in [19]. This yields:

$$V_h(q,z) = \frac{-e}{2\epsilon\sqrt{4a_B^{-2}+q^2}}\left(1 + \frac{2a_B^{-2}}{4a_B^{-2}+q^2} + \frac{2a_B^{-2}}{\sqrt{4a_B^{-2}+q^2}}|z|\right) \times exp\left(-\sqrt{4a_B^{-2}+q^2}\,|z|\right) \tag{9}$$

where $a_B = (4\pi\epsilon\hbar^2)/(m_\Gamma e^2)$ is the effective Bohr radius. From this potential, the screened scattering matrix elements can be computed the same way as for other mechanisms. The resulting mobility for an uniform distribution of NIs in GaN is shown in Fig. 4. At low n_s, the calculations tend to Erginsoy model but increasing n_s enhances screening and reduces the effect of background NIs (NIs located below the channel), leading to an increased mobility. In the following calculations, we will consider an inhomogeneous distribution of NIs.

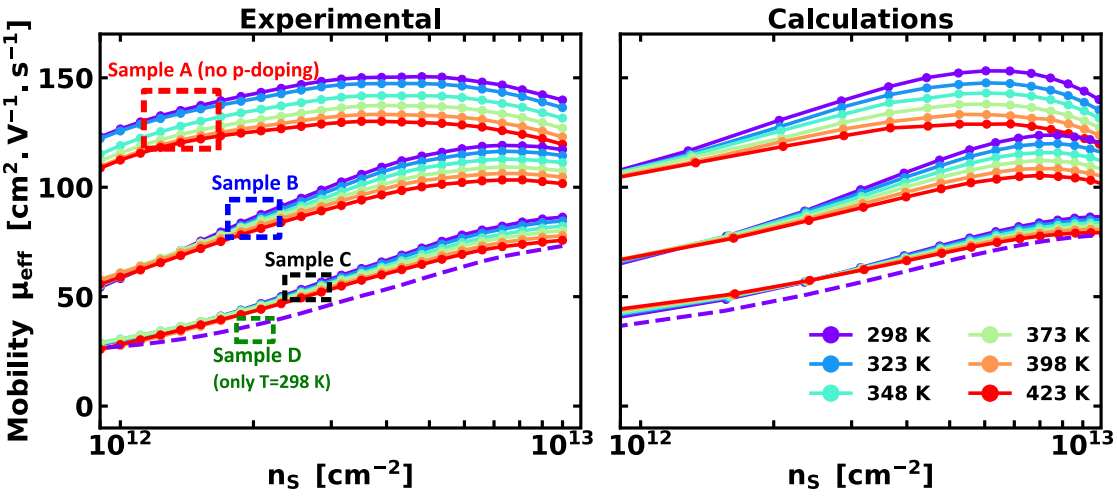

Fig. 6. μ_{eff} vs n_s from 298 K to 423 K (Experimental (left) and calculations (right)). In the calculations we used: a density of interface charges $\sigma_{Al_2O_3/GaN} = 1.42 \cdot 10^{13}$ cm^{-2}, a Gaussian distribution of neutral impurities centered at Al_2O_3/GaN interface with an integrated density $N_n^s = 7 \cdot 10^{12}$ cm^{-2} and for interface roughness, we employed an exponential spectrum with a correlation length $\Lambda_{sr} = 1.5$ nm and a root-mean-square $\Delta_{sr} = 0.6$ nm. These parameters are not changed between samples. $N_A(z)$ profiles in Fig. 1b are used in the calculations.

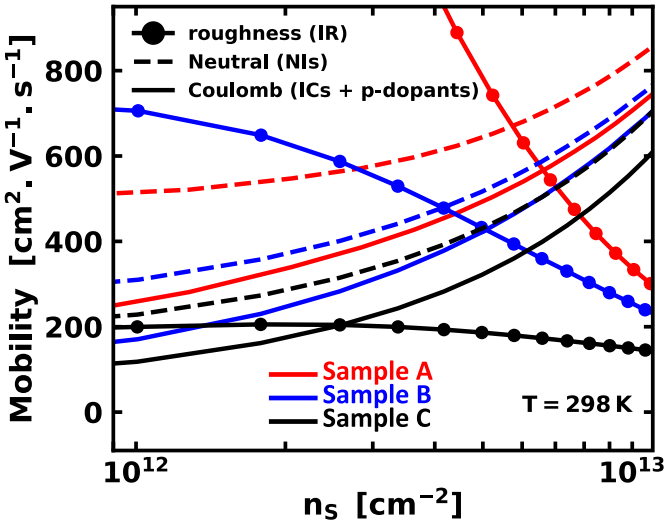

Fig. 7. Interface roughness, Coulomb and neutral impurities scattering limited mobility vs n_s for samples A, B, C. Increasing the level of p-doping and its proximity to the interface induces more confinement and enhances the effects of these scatterings. $N_A(z)$ profiles in Fig. 1b are used in the calculations.

4. Comparison with experiments

In Fig. 6(left), the experimental effective mobility μ_{eff} is plotted against n_s at different temperatures in the four samples. The only way to account for the low effective mobility and for the detrimental effect of p-doping on the mobility is by reinforcing scattering mechanisms located near the interface. Among those are ICs and IR scattering. A high ICs density with the same sign would induce a high V_{TH} shift. Alternative defects which do not affect the V_{TH} are NIs, hence we assume a part of the defects located near the interface to be NIs. A Gaussian distribution of NIs centered at Al_2O_3/GaN interface and with a standard deviation $\sigma = 1.5$ nm has been considered in the calculations. In Fig. 6, μ_{eff} vs n_s is calculated from 298 K to 423 K for the four samples and is compared to experimental measurements. With the same set of parameters, a good agreement is obtained for all samples, especially at high n_s but a high density of ICs and NIs was required to account for the low value of μ_{eff}. The ICs/NIs proportion can be modified without significantly changing the results. By bringing p-dopants closer to the interface (see $N_A(z)$ in Fig. 1b), μ_{eff} decreases because, as shown in Fig. 5, electrons are closer to Al_2O_3, thereby increasing the effect of IR, ICs and NIs. This is demonstrated in Fig. 7 where the mobility limited by these scattering mechanisms is shown for 3 samples. We can notice that p-doping has a huge impact on IR limited mobility especially as n_s decreases. In sample A, IR limited mobility is important mostly at high n_s, while in sample C, it is important in the whole n_s range. This is because, as depicted in Fig. 5, at low n_s, the electron channel of sample A is away from the interface and then, at high n_s, it gets much closer to the interface due to the high gate voltage applied. In contrast, in sample C, the electron channel is always confined and close to the interface (both at high and low n_s) due to the high level of p-doping. This is why the IR limited mobility of sample C is important in the whole n_s range. However, IR limited mobility cannot explain on its own the reduction in mobility induced by p-doping. ICs and NIs limited mobilities are also reduced by p-doping and their effect on transport is important, especially at low n_s (see Fig. 7). The Coulomb and neutral defects scattering is mostly due to the high density of interface defects (ICs and NIs). The scattering by p-dopants is negligible compared to the scattering due to interface charges.

5. Conclusion

The mobility in Al_2O_3/GaN channel was calculated while varying the proximity of GaN p-doping to the interface. The overall good agreement between calculations and experimental data on various samples strongly suggests that the transport limitations mostly come from interface roughness and from "defects" located near Al_2O_3/GaN interface. We illustrated the effect of interface charges and neutral impurities in this study but the exact origin of these "defects", most likely due to the high-κ Al_2O_3 oxide, needs to be further investigated.

Declaration of competing interest

The authors declare that they have no known competing financial interests or personal relationships that could have appeared to influence the work reported in this paper.

Data availability

Data will be made available on request.

Acknowledgment

This study was funded by the French national program "Programme d'Investissements d'Avenir PSPC No. 9 – G-Mobility, France".

References

[1] Amano H, Baines Y, Beam E, et al. The 2018 GaN power electronics roadmap. J Phys D: Appl Phys 51(16):163001. http://dx.doi.org/10.1088/1361-6463/aaaf9d.

[2] Rrustemi B, Viey AG, Jaud M-A, Triozon F, Vandendaele W, Leroux C, Cluzel J, Martin S, Le Royer C, Gwoziecki R, Modica R, Iucolano F, Gaillard F, Poiroux T, Ghibaudo G. Reliable method for low field temperature dependent mobility extraction at Al2O3/GaN interface. In: ESSDERC 2021 - IEEE 51st European solid-state device research conference. p. 295–8. http://dx.doi.org/10.1109/ESSDERC53440.2021.9631766.

[3] Bulutay C, Ridley BK, Zakhleniuk NA. Full-band polar optical phonon scattering analysis and negative differential conductivity in Wurtzite GaN. Phys Rev B 62(23):15754–63. http://dx.doi.org/10.1103/PhysRevB.62.15754.

[4] Jin S, Fischetti MV, Tang T-w. Modeling of electron mobility in gated silicon nanowires at room temperature: Surface roughness scattering, dielectric screening, and band nonparabolicity. J Appl Phys 102(8):083715. http://dx.doi.org/10.1063/1.2802586.

[5] Koller C, Lymperakis L, Pogany D, Pobegen G, Ostermaier C. Mechanism leading to semi-insulating property of carbon-doped GaN: Analysis of donor acceptor ratio and method for its determination. J Appl Phys 130(18):185702. http://dx.doi.org/10.1063/5.0060912.

[6] Koller C, Pobegen G, Ostermaier C, Huber M, Pogany D. The interplay of blocking properties with charge and potential redistribution in thin carbon-doped GaN on n-doped GaN layers. Appl Phys Lett 111(3):032106. http://dx.doi.org/10.1063/1.4993571.

[7] Tanaka T, Watanabe A, Amano H, Kobayashi Y, Akasaki I, Yamazaki S, Koike M. P-type conduction in Mg-doped GaN and Al0.08Ga0.92N grown by metalorganic vapor phase epitaxy. Appl Phys Lett 65(5):593–4. http://dx.doi.org/10.1063/1.112309.

[8] Fischetti MV. Long-range Coulomb interactions in small Si devices. Part II. effective electron mobility in thin-oxide structures. J Appl Phys 89(2):1232–50. http://dx.doi.org/10.1063/1.1332424.

[9] Esseni D, Palestri P, Selmi L. Nanoscale MOS transistors: Semi-classical transport and applications. Cambridge University Press.

[10] O'Regan TP, Fischetti MV, Sorée B, Jin S, Magnus W, Meuris M. Calculation of the electron mobility in III-V inversion layers with high-k dielectrics. J Appl Phys 108(10):103705. http://dx.doi.org/10.1063/1.3500553.

[11] Berdalovic I, Poljak M, Suligoj T. A comprehensive model and numerical analysis of electron mobility in GaN-based high electron mobility transistors. J Appl Phys 129(6):064303. http://dx.doi.org/10.1063/5.0037228.

[12] Fischetti MV, Neumayer DA, Cartier EA. Effective electron mobility in si inversion layers in metal–oxide–semiconductor systems with a high-k insulator: The role of remote phonon scattering. J Appl Phys 90(9):4587–608. http://dx.doi.org/10.1063/1.1405826.

[13] Bernardini F, Fiorentini V, Vanderbilt D. Polarization-based calculation of the dielectric tensor of polar crystals. Phys Rev Lett 79(20):3958–61. http://dx.doi.org/10.1103/PhysRevLett.79.3958.

[14] Ruf T, Serrano J, Cardona M, Pavone P, Pabst M, Krisch M, D'Astuto M, Suski T, Grzegory I, Leszczynski M. Phonon dispersion curves in Wurtzite-structure GaN determined by inelastic X-ray scattering. Phys Rev Lett 2022;86(5):906–9. http://dx.doi.org/10.1103/PhysRevLett.86.906.

[15] Yatabe Z, Hori Y, Ma W-C, Asubar JT, Akazawa M, Sato T, Hashizume T. Characterization of electronic states at insulator/(Al)GaN interfaces for improved insulated gate and surface passivation structures of GaN-based transistors. Jpn J Appl Phys 53(10):100213. http://dx.doi.org/10.7567/JJAP.53.100213.

[16] Perevalov TV, Shaposhnikov AV, Gritsenko VA, Wong H, Han JH, Kim CW. Electronic structure of α-Al2O3: Ab initio simulations and comparison with experiment. JETP Lett 85(3):165–8. http://dx.doi.org/10.1134/S0021364007030071.

[17] Frederick BG, Apai G, Rhodin TN. Surface phonons in thin aluminum oxide films: Thickness, beam-energy, and symmetry-mixing effects. Phys Rev B 44(4):1880–90. http://dx.doi.org/10.1103/PhysRevB.44.1880.

[18] Erginsoy C. Neutral impurity scattering in semiconductors. Phys Rev 79(6):1013–4. http://dx.doi.org/10.1103/PhysRev.79.1013.

[19] Ouisse T. Stationary occupied state in a Coulomb potential with electron screening. J Phys Soc Jpn 67(12):4157–63. http://dx.doi.org/10.1143/JPSJ.67.4157.